Taylor & Francis
Taylor & Francis Group

# Comparative analysis of daytime fire detection algorithms using AVHRR data for the 1995 fire season in Canada: perspective for MODIS

C. ICHOKU[1]*, Y. J. KAUFMAN[2], L. GIGLIO[1], Z. LI[3]†, R. H. FRASER[3], J.-Z. JIN[3]† and W. M. PARK[3]

[1]Science Systems and Applications Inc., NASA Goddard Space Flight Center, Code 913, Greenbelt, MD 20771, USA
[2]Laboratory for Atmospheres, NASA Goddard Space Flight Center, Code 913, Greenbelt, MD 20771, USA
[3]Natural Resources Canada, Canada Centre for Remote Sensing, 588 Booth St., Ontario, K1A OY7, Canada

**Abstract.** Two fixed-threshold (CCRS and ESA) and three contextual (GIGLIO, IGBP, and MODIS) algorithms were used for fire detection with Advanced Very High Resolution Radiometer (AVHRR) data acquired over Canada during the 1995 fire season. The CCRS algorithm was developed for the boreal ecosystem, while the other four are for global application. The MODIS algorithm, although developed specifically for use with the MODIS sensor data, was applied to AVHRR in this study for comparative purposes. Fire detection accuracy assessment for the algorithms was based on comparisons with available 1995 burned area ground survey maps covering five Canadian provinces. Overall accuracy estimations in terms of omission (CCRS = 46%, ESA = 81%, GIGLIO = 75%, IGBP = 51%, MODIS = 81%) and commission (CCRS = 0.35%, ESA = 0.08%, GIGLIO = 0.56%, IGBP = 0.75%, MODIS = 0.08%) errors over forested areas revealed large differences in performance between the algorithms, with no relevance to type (fixed-threshold or contextual). CCRS performed best in detecting real forest fires, with the least omission error, while ESA and MODIS produced the highest omission error, probably because of their relatively high threshold values designed for global application. The commission error values appear small because the area of pixels falsely identified by each algorithm was expressed as a ratio of the vast unburned forest area. More detailed study shows that most commission errors in all the algorithms were incurred in non-forest agricultural areas, especially on days with very high surface temperatures. The advantage of the high thresholds in ESA and MODIS was that they incurred the least commission errors. The poor performance of the algorithms (in terms of omission errors) is not only due to their quality but also to cloud cover, low satellite overpass frequency, and the saturation of AVHRR channel 3 at about 321 K. Great improvement in global fire detection can probably be achieved by exploring the use of a wide variety of channel combinations from the data-rich MODIS instruments. More sophisticated algorithms should be designed to accomplish this.

## 1. Introduction

Wild fires are a prominent global phenomenon, which not only destroy natural vegetation, but also pose enormous danger to wildlife as well as to human life and property. In addition, biomass burning by fires has been identified as a significant source of aerosols, carbon fluxes, and trace gases, which pollute the atmosphere and contribute to radiative forcing responsible for global climate change. In recent years, rapid deforestation occurred in the tropics due to human expansion and other developmental factors (Andreae *et al.* 1994). The situation is exacerbated by the increasing incidence of fires, which may have an adverse impact on the global environment.

Timely and accurate detection of fires has become an issue of considerable importance. Various international organizations, such as the International Geosphere and Biosphere Program (IGBP), have recognized the need for fire detection and monitoring (Giglio *et al.* 1999). The most feasible and practical methods of regional and global active fire detection rely on satellite data. However, owing to logistical and other technical factors, satellite data usually have certain limitations in meeting adequate spatial and temporal resolution requirements for effective fire detection. High spatial resolution satellite data, such as Landsat Thematic Mapper (TM), with 30 m pixel size, offer limited spatial coverage and revisit frequency (such that most parts of the world are imaged at best only once every 16 days). On the other hand, geostationary satellites, which acquire data several times a day over a given area, cover only a portion of the Earth in the low to mid latitudes, and their data generally have very low spatial resolution (4 km pixel size or larger). Until now, most fire detection activities have been based on the use of data from the Advanced Very High Resolution Radiometer (AVHRR) onboard the National Oceanic and Atmospheric Administration's (NOAA) polar orbiting satellites. The AVHRR series of sensors offer a spatial resolution of 1 km and cover most of the Earth's surface every day, once in the daytime and once at night. AVHRR data have been widely used for fire detection because they have some unique radiometric advantages relative to other satellite data (Li *et al.* 2001), and provide a good balance in spatial and temporal resolutions. More recently, the Moderate Resolution Imaging Spectroradiometer (MODIS) was launched onboard the Terra spacecraft on 18 December 1999. MODIS covers most of the Earth twice a day: once during the daytime and once at night. Another MODIS was launched onboard the Aqua spacecraft on 4 May 2002. Together, MODIS on Terra and Aqua cover all parts of the Earth at least four times a day (twice during the day and twice during the night), and more frequently in the high latitudes where many areas fall in the overlap of ground swaths. MODIS has 36 spectral channels in three spatial resolutions: 250 m at two channels (red and near infrared (NIR)), 500 m at five channels (going from blue to short wave infrared (SWIR)), and 1 km at the remaining 29 channels (ranging from blue to thermal infrared (TIR)). MODIS data offer a larger dynamic range of radiance values (12-bit quantization) than AVHRR data (10-bit quantization), thereby avoiding or lessening the saturation problem that has plagued fire detection with AVHRR. Fire is one of the operational standard products generated from MODIS, which shows great potential for global fire detection and monitoring.

Several algorithms have been developed for fire detection, mostly with AVHRR data (e.g. Kaufman *et al.* 1990, Arino *et al.* 1993, Justice *et al.* 1993, 1996, Justice and Dowty 1994, Kennedy *et al.* 1994, Franca *et al.* 1995, Flasse and Ceccato 1996, Justice and Malingreau 1996, Pozo *et al.* 1997, Rauste *et al.* 1997, Giglio *et al.* 1999,

Nakayama *et al.* 1999, Li *et al.* 2000a, Cuomo *et al.* 2001). The principles and limitations of the AVHRR-based fire detection algorithms were recently reviewed by Li *et al.* (2001). There have also been appreciable attempts to accomplish fire detection with other satellite data, including those of the Geostationary Operational Environmental Satellites (GOES) (e.g. Prins and Menzel 1992), the Visible and Infrared Scanner (VIRS) aboard the Tropical Rainfall Mapping Mission (TRMM) (e.g. Giglio *et al.* 2000), and MODIS on Terra (e.g. Kaufman *et al.* 1998, Justice *et al.* 2002). Some of the algorithms have been used for routine fire detection by different organizations. However, when applied to the same data set, they yield rather different results (Li *et al.* 2001). This can be very confusing to users of the products and policy makers, with damaging consequences. In this study, to quantify the differences between these algorithms, we have applied five standard fire detection algorithms to AVHRR data acquired over Canada during the 1995 fire season. The aim is to identify the strong and weak points of each algorithm, assess the data quality, and propose suggestions for improvement.

## 2. Data and algorithms

The main components of active fire remote sensing comprise the remotely sensed (e.g. AVHRR) data and the algorithm used to detect fire pixels from the data.

### 2.1. *Remote sensing data*

AVHRR has five spectral channels (bands) typically referred to as bands 1 to 5, and centered on 0.65, 0.86, 3.8, 10.8, and 11.9 $\mu$m wavelengths. With reference to the electromagnetic spectrum, bands 1 and 2 are in the visible and near-infrared (NIR) regions, respectively, band 3 in the mid infrared (MIR), and band 4 and 5 in the thermal infrared (TIR). MODIS has 36 spectral bands, ranging in wavelength from 0.405 to 14.385 $\mu$m, five of which are equivalent to those of AVHRR. Fire, because of its high temperature, emits thermal radiation with a peak in the MIR region, in accordance with Planck's theory of blackbody radiation (e.g. Serway 1992). Therefore, fire sensing is often done with data in the MIR to TIR (usually around 3.7 to 11 $\mu$m), although other spectral bands (mainly in the visible and NIR) may play complementary roles, such as for distinguishing fires from other features, including smoke and particles emitted by fires.

Conventionally, though not always, before fire detection, image radiance values in the MIR and TIR bands are converted to brightness temperatures. Also, where applicable, radiance values in the visible/NIR regions of the electromagnetic spectrum are first converted to reflectance. Subsequently, a fire algorithm is used to flag pixels that qualify as fire, based on the levels of their brightness temperatures and reflectance. Table 1 lists symbols designating the different variables used in this paper for fire detection with AVHRR.

### 2.2. *Fire detection algorithms*

In general, fire algorithms are classified as either 'fixed threshold' or 'contextual' (Justice and Dowty 1994). In the first category, a pixel is flagged as containing fire if the value of its brightness temperature and/or reflectance in one or more spectral bands (or combinations thereof) exceeds or falls below a certain predetermined threshold value. In the case of contextual algorithms, detection is based on the value of the candidate pixel in association with certain statistics of its neighbours, representing the background. Boles and Verbyla (2000), using some existing algorithms,

Table 1.   Glossary of variables used in the algorithms.

| Variable | Description |
| --- | --- |
| $R_1$ | Channel 1 (0.65 $\mu$m) AVHRR reflectance |
| $R_2$ | Channel 2 (0.86 $\mu$m) AVHRR reflectance |
| $T_3$ | Channel 3 (3.8 $\mu$m) AVHRR brightness temperature |
| $T_4$ | Channel 4 (10.8 $\mu$m) AVHRR brightness temperature |
| $T_5$ | Channel 5 (11.9 $\mu$m) AVHRR brightness temperature |
| $T_{3-4}$ | $T_3 - T_4$ |
| $T_{4-5}$ | $T_4 - T_5$ |
| $T_{3B}$ | $T_3$ for background pixels |
| $T_{4B}$ | $T_4$ for background pixels |
| $T_{5B}$ | $T_5$ for background pixels |
| $T_{3B-4B}$ | $T_{3B} - T_{4B}$ |
| $T_{4B-5B}$ | $T_{4B} - T_{5B}$ |
| $T_x$ | any one of $T_{3B}$, $T_{4B}$, $T_{5B}$, $T_{3B-4B}$, or $T_{4B-5B}$ specified |
| $\mu T_x$ | average (arithmetic mean) of $T_x$ |
| $\eta T_x$ | median of $T_x$ |
| $\delta T_x$ | mean absolute deviation of $T_x$ |
| $\sigma T_x$ | standard deviation of $T_x$ |
| MIN$\{...\}$ | the smallest of the list of arguments within the braces |
| MAX$\{...\}$ | the largest of the list of arguments within the braces |

derived an algorithm each to represent the 'threshold', 'contextual', and 'fuel mask' (a variant of the contextual) categories, and investigated their performance for fire detection in Alaska.

Five of the most prominent fire algorithms were implemented in this investigation, and have been identified by the name or acronym of the person(s), organization, or project, with which (whom) they are associated, as follows:

(a)  CCRS—algorithm developed and employed by the Canada Centre for Remote Sensing (CCRS) for operational fire detection in Canada (Li *et al.* 2000a).

(b)  ESA—algorithm used by the European Space Agency (ESA) in its operational fire detection program (Arino *et al.* 1993).

(c)  GIGLIO—algorithm developed and published by Giglio *et al.* (1999).

(d)  IGBP—algorithm used by the International Geosphere and Biosphere Project (IGBP) in its operational program (Justice *et al.* 1993, 1996, Justice and Dowty 1994, Flasse and Ceccato 1996).

(e)  MODIS—the operational MODIS algorithm (Kaufman *et al.* 1998: note that this is the only one of these algorithms developed for MODIS rather than AVHRR).

Table 2 summarizes the main features of these algorithms. Although daytime and night-time tests may be similar for some of the algorithms, the thresholds differ, and table 2 shows only daytime values. The components of each algorithm are listed according to their functionality:

(i)  *Potential fire detection:* The initial set of tests based on simple thresholds to identify potential fire pixels. Final fire detection involves further tests on the potential fire pixels (and, in the case of contextual algorithms, statistics of their neighbours).

(ii)  *Background selection:* Identifying neighbouring pixels that qualify for inclusion in the background sample for contextual algorithms. The search window

Table 2. Comparative summary of the five fire algorithms.

| Function | | CCRS (fixed thresholds, regional (Canada)) | ESA (fixed thresholds, global/ regional) | IGBP (contextual, global) | GIGLIO (contextual, global) | MODIS (contextual, global) |
|---|---|---|---|---|---|---|
| (i) | Potential fire detection | | | $T_3 > 311$ AND $T_{3-4} > 8$ | $T_3 > 310$ AND $T_{3-4} > 6$ | $T_3 \geqslant 315$ AND $T_{3-4} \geqslant 5$ |
| (ii) | Background selection | | | $T_3 \leqslant 311$ OR $T_{3-4} \leqslant 8$ | $T_3 \leqslant 318$ OR $T_{3-4} \leqslant 12$ | $T_3 \leqslant 320$ OR $T_{3-4} < 20$ |
| | Background window size | | | Growing from $3 \times 3$ to $15 \times 15$ | Growing from $5 \times 5$ to $21 \times 21$ | Growing from $3 \times 3$ to $21 \times 21$ |
| | Minimum number of pixels | | | MAX{25% of pixels tested, 3} | MAX{25% of pixels tested, 6} | MAX{25% of pixels tested, 3} |
| (iii) | Main fire detection (with $T_3$ AND/OR $T_4$) | $T_3 > 315$ | $T_3 > 320$ | Define: $\xi_3 = \mu T_{3B} + 2\sigma T_{3B} + 3$ | Define: $\xi_4 = \mu T_{4B} + \delta T_{4B} - 3$ | Define: $\xi_3 = $ MIN{320, $\mu T_{3B} + 4*$MAX$\{\sigma T_{3B}, 2\}\}$ |
| | | | | $\xi_{3-4} = $ MAX{8, $\mu T_{3B-4B} + 2\sigma T_{3B-4B}$} | $\xi_{3-4} = \mu T_{3B-4B} + $ MAX$\{2.5\delta T_{3B-4B}, 4\}$ | $\xi_{3-4} = $ MIN{20, $\eta T_{3B-4B} + 4*$MAX$\{\sigma T_{3B-4B}, 2\}\}$ |
| | | | | Then, flag as fire if: $T_3 > \xi_3$ AND $T_{3-4} > \xi_{3-4}$ | Then, flag as fire if: $T_4 > \xi_4$ AND $T_{3-4} > \xi_{3-4}$ | Then, flag as fire if: $T_3 > 360$ OR $[T_3 > \xi_3$ AND $T_{3-4} > \xi_{3-4}]$ |
| (iv) | Filter hot surfaces | $T_{3-4} \geqslant 14$ | $T_{3-4} > 15$ | *Incorporated in fire detection (iii)* | *Incorporated in fire detection (iii)* | *Incorporated in fire detection (iii)* |
| (v) | Filter clouds | $T_4 \geqslant 260$ | $T_4 > 245$ | Clear (not cloudy) pixel if: $\|R_1 + R_2\| \leqslant 1.2$ AND $T_5 \geqslant 265$ AND ($\|R_1 + R_2\| \leqslant 0.8$ OR $T_5 \geqslant 285$) | IGBP criteria applied here (no external cloud mask) | IGBP criteria applied here (no external cloud mask) |
| (vi) | Filter reflective surfaces | $R_2 \leqslant 0.22$ | $R_1 < 0.25$ | $R_2 < 0.20$ | $R_2 < 0.25$ | |
| (vii) | Filter sun glint | | $\|R_1 - R_2\| > 0.01$ | | | $R_1 \leqslant 0.3$ OR $R_2 \leqslant 0.3$ OR reflected sun angle $\geqslant 40°$ |
| (viii) | Other detection criteria | $T_{3-4} \geqslant 19$ OR $T_{4-5} < 4.1$ | | | | |
| (ix) | Post processing (not applied in this investigation) | $\Rightarrow$Elimination of non-forest and isolated pixels | $\Rightarrow$Quicklook inspection $\Rightarrow$Max. annual NDVI $> 0$ | | | |

Note: All temperature values are expressed in degrees Kelvin (K); all thresholds refer to daytime detection.

size grows until the minimum number of pixels required to constitute suffi-cient background sample is found, or until the maximum preset window size is reached.

(iii) *Main fire detection:* Tests to confirm whether a candidate pixel is likely to be true fire.

(iv) *Filter hot surfaces:* Tests to eliminate high temperature surfaces that most probably are not fire.

(v) *Filter clouds*: Filter pixels likely to be cloudy.

(vi) *Filter reflective surfaces:* Test to eliminate pixels that, because of high reflectivity, could be misclassified as fire pixels.

(vii) *Filter Sun glint:* Eliminates pixels affected by sun glint due to specular reflection, which occurs when the satellite view angle to a given pixel equals the solar zenith angle.

(viii) *Other detection criteria:* Some of the algorithms employ other complementary tests to improve the accuracy of the detection.

(ix) *Post processing:* Post-detection checks applied in some algorithms. Being often manual processes, they were not applied in this investigation.

## 3. Methodology: the Canadian experience

This section describes the AVHRR data used, data preprocessing and calibration, as well as algorithm implementation and fire detection.

### 3.1. *The AVHRR data*

The NOAA-14 AVHRR data used for this investigation cover the period from 1 May 1995 to 31 October 1995 (6 months), considered to be the fire season in Canada. The choice of 1995 was based on a previous investigation (Li *et al.* 2000a), which revealed that, over the period 1994 to 1998, the year 1995 had the largest concentration of fire activities in Canada. Canadian forest fire agencies reported that 7.1 million ha of forest burned that year (http://nfdp.ccfm.org/). Furthermore, over that 5-year period, 1995 had the largest amount of validation information obtained by provincial and local fire authorities (Li *et al.* 2000b).

For this study, only daytime images were used. Individual image frames for each day were merged to create a mosaic covering almost the entirety of Canada (Li *et al.* 2000a). The mosaic consists of 4800 rows by 5700 columns of pixels, making a total of 27 360 000 pixels.

### 3.2. *Data calibration and quantization*

The calibration was done differently for the solar (1 and 2) and thermal (3 to 5) channels. Because of the lack of on-board calibration facilities for solar channels, post-launch vicarious calibration was applied to AVHRR channels 1 and 2, to account for the post-lunch sensor degradation. A piece-wise linear calibration method (Cihlar and Teillet 1995) was employed together with time-dependent calibration coefficients provided by NOAA (Rao and Chen 1996):

$$L_{TOA} = \frac{DN - O}{G} \tag{1}$$

$$G = A \times days\ from\ launch + B \tag{2}$$

$$O = C \times days\ from\ launch + D \tag{3}$$

where $DN$ is the raw counts from the sensor; $L_{TOA}$ is the top of the atmosphere (TOA) Radiance (in W/m$^2$/sr/$\mu$m); $G$ is calibration gain coefficient (counts/radiance);

$O$ is calibration offset coefficient (counts); $A$, $B$, $C$, and $D$ are time-dependent piecewise linear (PWL) calibration coefficients. Since the PWL method employs a second order polynomial and limited calibration data, some uncertainties are associated with both the source calibration data/methodology and the polynomial fit. The absolute calibration errors for the solar channels are estimated to be $\pm 6\%$ at best (Cihlar *et al.* 2001).

The AVHRR thermal data (channels 3, 4 and 5) were calibrated on-board by observing the onboard internal calibration target (ICT) signal $C_{ICT}$ and the deep-space (SP) signal $C_{SP}$ (Kidwell 1998). Radiance from the ICT ($R^{(i)}_{ICT}$) at a given temperature $T_{ICT}$ is computed by integrating the Planck's function over a spectral band $i$. Four platinum resistance thermometers (PRTs) are employed to measure $T_{ICT}$. The calibration gain $G^{(i)}$ and offset $I^{(i)}$ are determined by

$$G^{(i)} = \frac{R^{(i)}_{ICT} - R^{(i)}_{SP}}{C^{(i)}_{TCT} - C^{(i)}_{SP}} \tag{4}$$

$$I^{(i)} = R^{(i)}_{SP} - G^{(i)} C^{(i)}_{SP} \tag{5}$$

A small non-zero radiance $R^{(i)}_{SP}$ is assigned to the SP signal to account for the non-linearity effect (Kidwell 1998). While extensive pre-launch calibration tests were carried out by NOAA and the temperature accuracy was quoted as $\pm 0.2 \deg K$, the actual performance of the sensor calibration may change from time to time especially when the satellite drifts into a later orbit where solar radiation may contaminate blackbody measurements. According to a recent study by Trishchenko and Li (2001), the contamination may incur an error of up to 0.6 K.

The implementation of the calibration and generation of the Canada-wide mosaic was carried out within the AVHRR GEOCOMP (geocoding and compositing) processing system (Robertson *et al.* 1992). Incidentally, the process employs the NOAA-11 AVHRR quantization coefficients. The result is that the upper bound of the dynamic range of NOAA-14 AVHRR data values (such as ours) is slightly truncated in channel 3. Thus, the saturation value of the brightness temperature in channel 3 became exactly 320.12 K, even though it was expected to be slightly higher. Considering that channel 3 is already plagued with early saturation, the truncation made this early saturation only infinitesimally worse. We investigated the effect that this would have on fire detection with our data and found it to be negligible. The data used in prior studies (Li *et al.* 2000 a,b) were calibrated and quantized in the same way.

### 3.3. *Fire detection*

Each of the five algorithms was coded in FORTRAN-77 and used to detect fire pixels from daily AVHRR mosaics of Canada. A landcover mask is used to identify only land (as opposed to water covered) pixels for processing. Figure 1 shows serial plots of the counts of clear land (non-water, non-cloudy) pixels as well as pixels flagged as fire by the various algorithms for each day of the experiment. Out of the total of over 27 million pixels in the mosaic, on most of the days, cloud-free land pixels numbered between 6 and 8 million. Generally, the IGBP algorithm consistently flagged the largest number of pixels daily. The CCRS and GIGLIO algorithms consistently flagged comparable numbers of pixels, though less than IGBP by a factor of 2, while ESA and MODIS flagged less than IGBP by a factor of 10. However, there seems to be a very appreciable correlation between the fire pixel
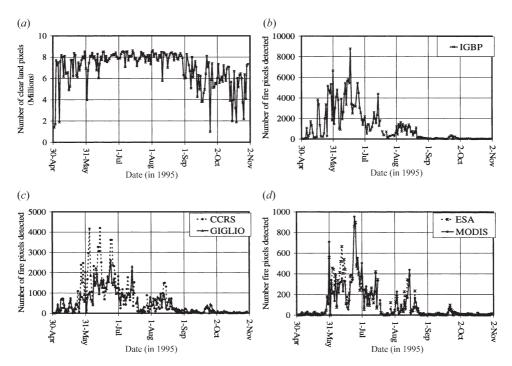
(a)

(b)

(c)

(d)

Figure 1. Counts of clear land (non-water, cloud-free) pixels as well as pixels flagged as fire by the five algorithms throughout Canada each day during the 1995 fire season. Notice the scale differences between the vertical axes.

counts from all algorithms. In fact, the correlation coefficients computed from these values range from 0.62 to 0.94, with the lower value (0.62) being between IGBP and MODIS, while the higher value (0.94) was between ESA and MODIS.

## 4. Analysis of results

The large discrepancy between the fire detection results of the different algorithms is quite alarming and calls for more in-depth investigation into the probable reasons. As such, we embarked on a detailed study of both the data and the algorithms. To achieve a balanced result analysis, it has been necessary to make use of reliable ground data (so-called 'ground truth').

### 4.1. *Validation with ground data*

The available ground data consisted of maps delineating the perimeters of burned areas. These maps provided by some Canadian provincial government authorities show cumulative burned areas for each entire calendar year (in this case 1995). The available 1995 perimeter maps cover five Canadian provinces/territories that experienced extensive burning, which affected 5.1 million ha or 72% of the national forest burned area. They were digitized and scaled to co-register with the AVHRR mosaics of Canada. Figure 2 shows a map of Canada with forested regions in the five provinces shaded in grey, while the 1995 burned areas mapped within these regions are shaded in black. One severe limitation of such cumulative annual burned-area maps is that they are temporally not precise enough to check individual fire events, which is what the assessment of the accuracy of detection aims to achieve. However,

those maps were the best ground information available, and in fact, are esteemed to be one of the best fire ground data available to date, globally speaking. Despite their limitations, the annual burned area maps have been very useful in guiding the fire detection accuracy evaluation.

A general assessment of the fire detection algorithms on an annual basis can be made by comparing the daily satellite-based fire masks composited over the 1995 fire season against the forest fire perimeter maps produced by provincial fire management agencies (figure 2). Errors of omission were calculated by dividing the total area within the reference fire polygons not mapped by each fire algorithm by the total area of the polygons. Overall commission error (i.e. proportion of incorrectly mapped fire pixels) within the five provinces was calculated by dividing the area of satellite fire pixels lying outside of the polygons by the total area of unburned forest. Since the provincial surveys provide extensive mapping of fires affecting forested areas only, the commission error was computed based on forested land cover types. This was accomplished using a mask of candidate forest areas created using an AVHRR-based land cover classification shown as grey-shaded regions in figure 2 (Pokrant 1991). Table 3 summarizes the composited area of fire pixels from each algorithm contained both within and outside the reference burned area polygons in



Figure 2. Map of Canada showing provincial boundaries. Burned area assessment was conducted in the five provinces with grey shaded areas, which represent forests. The dark areas within the forested regions are the 1995 burned areas mapped by the five Canadian provincial/territorial fire management agencies. The prominent star at the lower-right corner of the province of Alberta marks the location of Medicine Hat, where the meteorological data plots shown in figure 3 were measured. It lies at the heart of the Canadian agricultural/prairie region, where most of the algorithms committed substantial false alarms.

Table 3. Summary of 1995 burned and non-burned forest areas using the cumulative pixel counts from the five satellite fire detection algorithms, based on the inclusion or exclusion of the fire pixels within the burned area polygons provided by the provincial land/fire management authorities.

| | Burned forest area (ha) and omission error (%) | Unburned forest area (ha) and absolute commission error (%) | Proportional commission error (%) |
|---|---|---|---|
| Total forest area | 5 092 600 (N/A) | 331 566 200† (N/A) | (N/A) |
| CCRS algorithm | 2 729 000 (46) | 1 175 700 (0.35) | 30 |
| ESA algorithm | 978 300 (81) | 263 700 (0.08) | 21 |
| GIGLIO algorithm | 1 287 100 (75) | 1 871 500 (0.56) | 59 |
| IGBP algorithm | 2 512 900 (51) | 2 535 300 (0.75) | 50 |
| MODIS algorithm | 972 100 (81) | 273 800 (0.08) | 22 |

†Extent of unburned forest area covered by ground surveys.
N/A = not applicable.

relation to the 'true' area of burned and non-burned forest within the five provinces (first row). Corresponding omission and commission errors are also presented in parentheses. Omission errors ranged from 46% for the CCRS algorithm to 81% for the MODIS algorithm. A certain proportion of burned areas may have been missed due to constraints not related to algorithm design, including limited satellite diurnal sampling and cloud cover (Li *et al.* 2000b). The (absolute) commission error was consistently small because it was based on the vast area of unburned forest (331 566 200 ha). Note that true commission errors can be larger than those shown in table 3 if other land cover types (apart from forest) are included because, as will be demonstrated later, large commission errors have been found to occur in the Canadian agricultural/prairie areas. Nevertheless, the potential error increase may be compensated to some extent due to possible omissions in the reference burned-area perimeter maps, as the fire surveys were found not to include some of the 1995 burned areas (Fraser *et al.* 2000). Furthermore, the coarse footprint provided by AVHRR (1.2–15 km$^2$) often causes single sub-pixel fires to cover several pixels after resampling to a 1 km grid. In many cases, this causes single hotspot sources related to a real fire event to fall outside the mapped fire perimeter. However, if the area misidentified by each algorithm is expressed as a ratio of the total area it identifies as fires, the ratio (referred to as 'proportional commission error' in table 3) is quite large, ranging from 21% for ESA to 59% for GIGLIO.

To evaluate the accuracy of fire detection in more detail, a few days were selected for closer examination. Validation data sets were extracted from the data representing these dates in the form of 'TRUE' and 'FALSE' fire masks. 'TRUE' fire masks were extracted for dates on which large fires were known to have occurred (e.g. 25 June 1995). A pixel was selected as 'true' fire if it satisfied the following three conditions: (i) it must fall within one of the perimeters of the burned-area maps for 1995; (ii) its channel 3 brightness temperature must be greater than 315 K ($T_3 > 315$, because this is the lowest temperature threshold used for fire detection among the algorithms), (iii) there must be an obvious smoke plume emanating from it. Based on the knowledge of fire characteristics in the areas studied, it is estimated that the maximum error incurred by this method of identification of true fire pixels is about 10%. For

25 June 1995, the total number of true fire pixels identified was 2043. 'FALSE' fire masks were extracted only from areas where fire seemed impossible to occur on given dates (e.g. 29 May 1995 in the prairie areas). Pixels selected as 'FALSE' fires are those flagged as fires by at least one of the algorithms. An example is the Canadian southern agricultural/prairie areas (unshaded area marked by a star in figure 2), where all the algorithms flagged fires on 29 May 1995. It was verified that there was no fire in those areas around that date, although the ground temperature was very high (see figure 3), which is probably the source of the false alarms. A total of 5130 pixels fall into this category for 29 May 1995.

To estimate the performance of each algorithm on any validation date, the actual ratio (%) of the total 'TRUE' or 'FALSE' fires flagged by that algorithm is calculated for that date. Figure 4 shows a bar chart of the 'TRUE' (25 June 1995) and 'FALSE' (29 May 1995) detection ratios, for the five algorithms. The CCRS algorithm detected the largest proportion of true fires, while the ESA and MODIS algorithms both detected the least proportion (i.e. produced the largest error of omission). The IGBP algorithm flagged the largest number of false fires (error of commission), and again the ESA and MODIS algorithms both produced the least error of commission. To test the robustness of this validation method, it was repeated for a few other dates ranging from several days to several weeks before and after the main fire event of 25 June 1995, on the exact same pixels used for the true fire of that date. For each of the dates chosen, pixels flagged before and after the fire event, though are false fires, shall be referred to as 'PRE' and 'POST' fires, respectively. This is to distinguish them from those specifically identified as 'FALSE' fires.

The PRE- and POST-fire data show very few to no pixels flagged before and after the fire event irrespective of algorithm. It can be said that for the forested areas
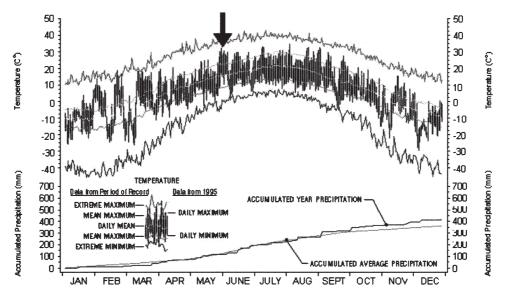


Figure 3.  The 1995 meteorological data time series for Medicine Hat (latitude 50° N, longitude 110.7° W), Alberta, Canada. The site lies at the heart of the Canadian agricultural/prairie region, where most of the algorithms committed substantial false alarms. Arrow on top shows the peak temperatures that occurred at the end of May 1995. In the analysis of the fire algorithms, data for 29 May 1995 in this region were used to demonstrate the false alarms.
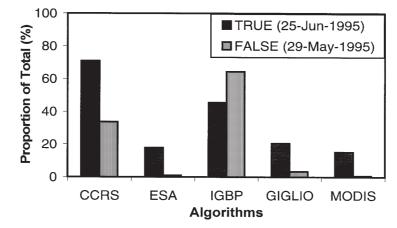
Figure 4. Percentage of total 'TRUE' or 'FALSE' fire pixels flagged as fire by each of the five algorithms.

tested, each algorithm flagged fire mainly during the fire event. This is an indication that the 'TRUE' fire validation criteria used here are appreciably reliable. The 'FALSE' fire validation is also very reliable, based on the fact that records obtained from local authorities ruled out any possibility of fires in the Canadian agricultural/prairie area under investigation on or around 29 May 1995.

### 4.2. *Analysis of the AVHRR data characteristics*

Virtually all tests in all the algorithms (whether fixed threshold or contextual) are based on the application of thresholds for individual parameters or background statistics thereof, or algebraic combinations of these. Therefore, it is essential to examine the values of these variables with a view to determining the applicable optimal thresholds, or even finding alternatives to the use of thresholds. As such, all the variables used for detection (as listed in table 1) in all the algorithms (table 2) have been computed for all the validation pixels and dates. To simplify analysis, the variables are binned into several value ranges and used to plot histograms, which show the statistical distribution of their values.

#### 4.2.1. *Pixel reflectances ($R_1$ and $R_2$)*

Figure 5 shows plots of histograms of $R_1$ and $R_2$ (red and NIR reflectance, respectively) for the 'TRUE', 'FALSE', 'PRE', and 'POST' cases. In most of the algorithms making use of $R_1$ or $R_2$, the values for fire are required to be below a certain threshold (CCRS: $R_2 \leqslant 0.22$; ESA: $R_1 < 0.25$; IGBP: $R_2 < 0.20$; GIGLIO: $R_2 < 0.25$). It is obvious from figure 5 that both fires and non-fires have the majority of their reflectance values below these thresholds. Therefore, no specific $R_1$ or $R_2$ threshold value or range of values appears to be peculiar to fires. Paradoxically, in figure 5(*a*) the 'TRUE' fire (25 June 1995) is the only case where the distribution of $R_1$ appears to be bimodal, extending slightly to higher values with respect to those of the non-fires. Therefore, the use of $R_1$, as in the ESA algorithm, can cause some real fires to be missed. To see if this could, however, lend some importance to the $R_1$–$R_2$ difference (used in the ESA algorithm), the distribution of $R_1 - R_2$ was examined, but again no specific range of values applies uniquely to true fires.
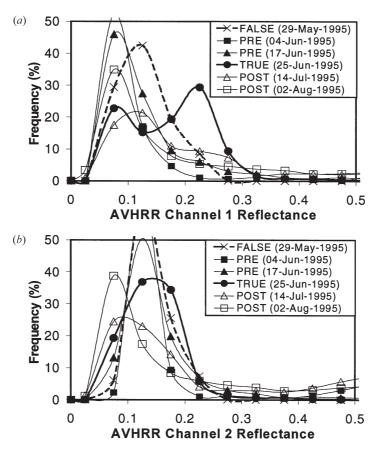
Figure 5.  Distribution of AVHRR channel 1 and channel 2 reflectances for the sample 'TRUE' (25 June 1995) and 'FALSE' (29 May 1995) fire dates, as well as for two dates each before ('PRE') and after ('POST') the 'TRUE' fire. The 'PRE' and 'POST' cases represent the exact same pixels as 'TRUE', but on different dates before and after the true fire, respectively.

### 4.2.2. *Pixel brightness temperatures (* $T_3$ *and* $T_4$ *)*

Brightness temperatures derived from AVHRR thermal channels, particularly channels 3 and 4 ($T_3$ and $T_4$), are the main parameters used in the actual fire detection. In four of the algorithms (CCRS, ESA, IGBP, and MODIS), the $T_3$ value for a fire candidate pixel is used as the main determinant for detection, while in the GIGLIO algorithm, although $T_3$ is also used in flagging potential fires, it is $T_4$ that is used in the final decision. However in all the algorithms, the value of the difference between these two channels (i.e. $T_3$–$T_4$) is considered to be of strategic importance in fire detection.

Figure 6 shows the distribution of the pixel $T_3$ for the 'TRUE' (25 June 1995) and 'FALSE' (29 May 1995) fire cases. Both have practically the same range of values, which are mostly 315 K or larger, and, if this is used as the only basis for fire detection, whatever threshold selected can cause large omission or commission errors or both. 'PRE' and 'POST' fire pixels, although not shown, have relatively low $T_3$ values (310 K or lower).
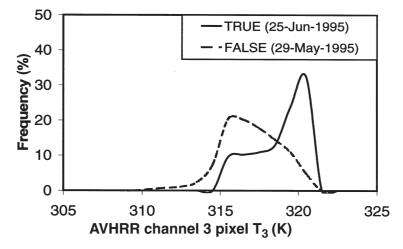
Figure 6.   Distribution of the AVHRR channel 3 brightness temperatures for the 'TRUE' fire
pixels on 25 June 1995 as against the 'FALSE' fires in the Canadian prairie areas on
29 May 1995.

The distribution of $T_4$ values was also analysed. The peak value for the 'TRUE'
fire case was 300 K, while that of 'FALSE' was 305 K. In fact, most of the peaks for
the 'PRE' and 'POST' cases fall between these two values. Therefore, the pixel $T_4$
value by itself does not provide a suitable basis for the application of a fixed
threshold.

In addition, the distribution of the spectral brightness temperature difference,
$T_{3-4}$ (i.e. $T_3-T_4$), was analysed, but there is no specific distinguishing pattern between
the real fire and non-fire cases.

### 4.2.3.  *Background brightness temperatures (* $T_3$ *and* $T_4$ *)*

The main difference between the fixed threshold (CCRS and ESA) and contextual
(GIGLIO, IGBP, and MODIS) algorithms is that, unlike the former, the latter
algorithms take the potential fire background into consideration in confirming a
fire. The background characteristics are evaluated from the average (mean or median)
and variation (mean absolute deviation or standard deviation) of their $T_3$, $T_4$, and
$T_{3-4}$ values.

Figure 7 shows the distributions of the mean $T_3$ ($\mu T_{3B}$) derived from background
pixels based on the IGBP and the MODIS selection methods. The distributions
produced by the two methods are almost identical in the 'PRE' and 'POST' fire
situations (figure 7(*b*)). But in the 'TRUE' and 'FALSE' fire cases (figure 7(*a*)), the
$\mu T_{3B}$ values generated using the MODIS selection criteria are markedly higher than
corresponding values derived through the IGBP background selection method. Also,
for IGBP the values for 'FALSE' are generally higher than 'TRUE', whereas for
MODIS they are almost within the same range. The effect of these distributions of
$\mu T_{3B}$ in the fire detection equations (table 2), given the corresponding distributions
of $T_3$ (figure 6), is that IGBP produces more commission errors while MODIS gives
more omission errors. This makes it difficult to choose one method of background
selection in preference to the other.

The mean background $T_4$ ($\mu T_{4B}$) was generated using only the GIGLIO selection
criteria, since it is the only algorithm that uses it for fire detection. Figure 8 shows
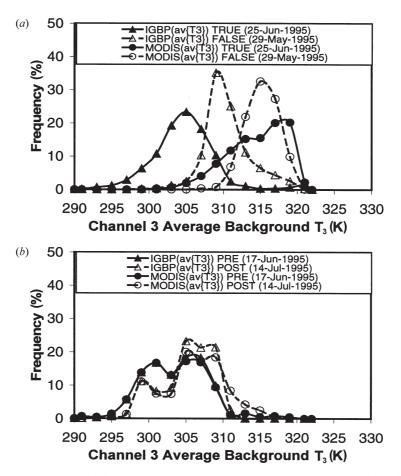
Figure 7. Distribution of fire background average brightness temperatures from AVHRR channel 3 (av{T3}), based on the criteria used by the IGBP and MODIS algorithms. They represent (*a*) the sample 'TRUE' (25 June 1995) and 'FALSE' (29 May 1995) fire dates, as well as (*b*) for a date each before ('PRE') and after ('POST') the 'TRUE' fire. The 'PRE' and 'POST' cases represent the exact same pixels as 'TRUE', but on different dates before and after the true fire, respectively.

$\mu T_{4B}$ and the candidate pixel $T_4$ plotted together for the 'TRUE' and 'FALSE' cases. Incidentally, the $T_4$ and $\mu T_{4B}$ distributions are related to each other for 'TRUE' fires in the same way as they are for 'FALSE' fires, both in shape and in relative location. $T_4$ and $\mu T_{4B}$ distributions for 'PRE' and 'POST' cases were also plotted, although not shown, and found to be almost coincident, especially for higher values. Therefore, the relationship between $T_4$ and $\mu T_{4B}$ does not appear to provide a strong enough basis to distinguish fires from non-fires.

The average background $T_{3-4}$ was calculated based on the background selection methods of IGBP, GIGLIO, and MODIS. Note that, instead of the mean ($\mu T_{3B-4B}$) used in the IGBP and GIGLIO methods, the background statistic used in the case of MODIS is the median ($\eta T_{3B-4B}$), which was found to be more robust than the mean for the type of distribution that $T_{3B-4B}$ generally presents. It was found that, for each date of 'PRE' and 'POST', the distributions for $T_{3-4}$ and $\mu T_{3B-4B}$ (or $\eta T_{3B-4B}$) coincide almost completely regardless of background selection method. In both the
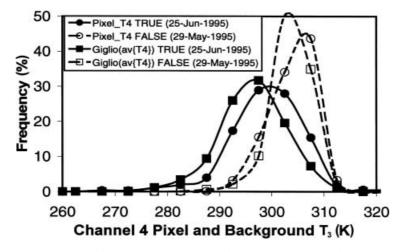
Figure 8. Distribution of brightness temperatures from AVHRR channel 4 for the candidate fire pixel (Pixel_T4) and its background average based on the GIGLIO algorithm criteria (av{T4}), for the sample 'TRUE' (25 June 1995) and 'FALSE' (29 May 1995) fire dates.

'TRUE' and 'FALSE' situations, the candidate pixel $T_{3-4}$ distributions show a slightly wider spread towards larger values than their corresponding $\mu T_{3B-4B}$ (or $\eta T_{3B-4B}$) distributions. Figure 9 shows, for instance, $\mu T_{3B-4B}$ for IGBP plotted alongside the pixel $T_{3-4}$ for the 'TRUE' and 'FALSE' cases. Although, in this case, the separation between the distributions of $T_{3-4}$ and $\mu T_{3B}$ for the 'TRUE' fires is fairly larger than that of 'FALSE', this is less so for the GIGLIO and MODIS methods. Therefore, the success of using $\mu T_{3B-4B}$ (or $\eta T_{3B-4B}$) depends on the background selection method and the threshold value chosen.

Measures of dispersion of the background $T_3$, $T_4$, and $T_{3-4}$, such as their standard deviations ($\sigma$) or mean absolute deviations ($\delta$), are also used to increase the efficacy of fire detection in the contextual algorithms. These quantities were computed accordingly for the different contextual algorithms for the validation dates. For each of the validation dates the distributions of the six variables are almost clustered together, except that all the distributions for 'TRUE' fires spread slightly towards higher values. In fact, 90–95% of the computed deviations fall in the range of 0 to 5 K for 'FALSE', 'PRE', and 'POST', while for 'TRUE', about 55–60% fall in that range and almost all the rest fall in the range of 5 to 9 K. Thus, it is unlikely that the dispersions of background $T_3$, $T_4$, and $T_{3-4}$, as used in the fire algorithms, provide a strong basis for distinguishing fires from non-fires. However, for the TRUE-fire case (25 June 1995) we found the GIGLIO-based $\delta T_{4B}$ tend towards lower values and the IGBP-based $\sigma T_{3B}$ tend towards higher values, with some overlap. Since this distribution difference was not present in any of the other three situations ('FALSE', 'PRE', and 'POST'), these two quantities potentially could be used together to detect real fires.

### 4.3. Detailed analysis of the algorithms

Each of the algorithms was broken down into its component unit tests. This is to characterize each one individually, and to determine if unit tests from different algorithms could be combined in such a way as to optimize fire detection. Table 4
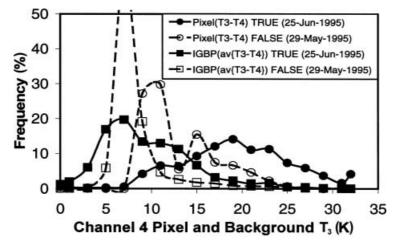
Figure 9. Distribution of brightness temperature differences between AVHRR channels 3 and 4 ($T_3$–$T_4$ or $T_{3-4}$) for the candidate fire pixel (Pixel(T3-T4)) and its background average (av{T3-T4}) based on the IGBP criteria ( just as illustration). They represent the sample 'TRUE' (25 June 1995) and 'FALSE' (29 May 1995) fire dates.

shows the breakdown of the tests, which are identified with the name of the algorithm to which they belong (CCRS, ESA, GIGLIO, IGBP, or MODIS), with serial numerical suffixes.

Figure 10 shows the ratio (in %) of the number of pixels that passed each individual test with respect to the total number of pixels (5130 for 'FALSE' and 2043 for 'TRUE', 'PRE', or 'POST'). Figure 10(*a*) compares the 'TRUE' and 'FALSE' cases, while figure 10(*b*) presents one each of the 'PRE' and 'POST' cases for comparison. This type of plot could be helpful in determining if there are any test combinations, irrespective of algorithm, that could produce optimal detection (with minimal omission and commission errors). Such would be tests for which the pass ratio is very high for 'TRUE' but very low for the other cases. Unfortunately, none of the tests clearly shows such a quality. All the tests that scored high for 'TRUE' also scored high for 'FALSE', and in some cases also for 'PRE' and 'POST'. Conversely, all the tests that scored low for 'FALSE', 'PRE', and 'POST', did not score high enough for 'TRUE'. Since similar tests from different algorithms use different thresholds, it is not obvious that there could be much improvement by adjusting thresholds. Rather, as has already been revealed from the data analysis above, a large part of the limitation in fire detection accuracy can be attributed to the limitation in the AVHRR data quality, such as the saturation of channel 3 at approximately 321 K.

Figure 10 can also enable the estimation of the omission or commission error that each test can potentially produce, if used alone for fire detection, or contribute to the algorithm within which it is used. If *P* denotes the pass ratio (in %), the potential error of commission for a given test is the largest value of *P* among the 'FALSE', 'PRE', or 'POST' categories, while the potential error of omission is the value of 100–*P* from the 'TRUE' category.

## 5. MODIS fire detection capability

From the forgoing analysis of current fire detection methods using AVHRR data, it is obvious that there are considerable issues to deal with, both in the data and in

Table 4. Individual tests of the five algorithms.

| Test ID | Test expression | Remarks |
|---|---|---|
| CCRS1 | $T_3 > 315$ | |
| CCRS2 | $T_{3-4} \geqslant 14$ | |
| CCRS3 | $T_4 \geqslant 260$ | |
| CCRS4 | $R_2 \leqslant 0.22$ | |
| CCRS5 | $T_{3-4} \geqslant 19$ | |
| CCRS6 | $T_{4-5} < 4.1$ | |
| ESA1 | $T_3 > 320$ | |
| ESA2 | $T_{3-4} > 15$ | |
| ESA3 | $T_4 > 245$ | |
| ESA4 | $R_1 < 0.25$ | |
| ESA5 | $|R_1 - R_2| > 0.01$ | |
| IGBP1 | IGBP background sufficiency test | |
| IGBP2 | $R_2 < 0.20$ | |
| IGBP3 | $T_3 > 311$ | |
| IGBP4 | $T_{3-4} > 8$ | |
| IGBP5 | $T_{3-4} > \xi_{3-4}$ | $\xi_{3-4} = \mathrm{MAX}\{(\mu T_{3B-4B} + 2\sigma T_{3B-4B}), 3\}$ |
| IGBP6 | $T_3 > \xi_3$ | $\xi_3 = \mu T_{3B} + 2\sigma T_{3B} + 3$ |
| GIGLIO1 | GIGLIO background sufficiency test | |
| GIGLIO2 | $T_3 > 310$ | |
| GIGLIO3 | $T_{3-4} > 6$ | |
| GIGLIO4 | $R_2 < 0.25$ | |
| GIGLIO5 | $T_{3-4} > \xi_{3-4}$ | $\xi_{3-4} = \mu T_{3B-4B} + \mathrm{MAX}\{4, 2.5\delta T_{3B-4B}\}$ |
| GIGLIO6 | $T_4 > \xi_4$ | $\xi_4 = \mu T_{4B} + \delta T_{4B} - 3$ |
| MODIS1 | MODIS background sufficiency test | |
| MODIS2 | $T_3 \geqslant 315$ | |
| MODIS3 | $T_{3-4} \geqslant 5$ | |
| MODIS4 | $T_3 > \xi_3$ | $\xi_3 = \mu T_{3B} + 4\mathrm{MAX}\{\sigma T_{3B}, 2\}$ |
| MODIS5 | $T_3 > 320$ | |
| MODIS6 | $T_{3-4} > \xi_{3-4}$ | $\xi_{3-4} = \eta T_{3B-4B} + 4\mathrm{MAX}\{\sigma T_{3B-4B}, 2\}$ |
| MODIS7 | $T_{3-4} > 20$ | |
| MODIS8 | $T_3 > 360$ | |

the algorithm, to reduce errors (omission and commission) and improve detection accuracy. It appears that the major problem is with the AVHRR data characteristics, as sophistication in algorithm development can be very heavily impaired by data limitations. MODIS has a great potential for fire detection in a dependable way. This is because MODIS has 36 spectral bands of which the five equivalent to those of the AVHRR have equal or better spatial resolution, saturation level, dynamic range, and signal-to-noise ratio than the corresponding AVHRR bands.

Fire is one of the standard products of MODIS. Incidentally, the original MODIS fire algorithm used in this study was developed on the basis of knowledge and concepts more compatible with AVHRR data than with MODIS data, since only the former (but not the latter) was in existence at the time of the development of the algorithm. However, the MODIS algorithm is currently being optimized based on real MODIS data and operational fire products are now being produced. Luckily, given the high quality of MODIS data, there is great potential for rapid advancement in MODIS fire detection. When most of the MODIS channels would have become
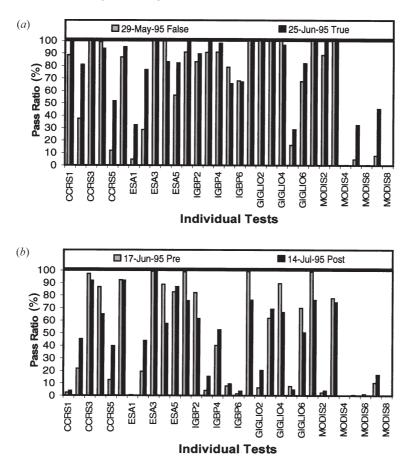
Figure 10. Comparison of pass ratios of the individual tests, identified by their algorithm names (with numeric suffixes, as in table 4) for the various validation dates, including (*a*) the 'TRUE' (25 June 1995) and 'FALSE' (29 May 1995), and (*b*) one each of the 'PRE', and 'POST' fire cases. This is to explore the possibility of combining individual tests from different algorithms to improve detection accuracy and reduce false alarms.

well calibrated and characterized, use can be made of other spectral bands instead of, or, in addition to the five channels corresponding to those of the AVHRR.

## 6. Conclusions

Five fire detection algorithms (CCRS, ESA, GIGLIO, IGBP, and MODIS) have been implemented and tested with AVHRR data acquired over Canada during the 1995 fire season (1 May to 30 September 1995). Overall accuracy estimates were obtained by comparing composited fire masks for the entire 1995 season against the 1995 total burned area maps produced by ground survey in five large provinces. The estimated omission errors were CCRS = 46%, ESA = 81%, GIGLIO = 75%, IGBP = 51%, MODIS = 81%, while the commission errors were CCRS = 0.35%, ESA = 0.08%, GIGLIO = 0.56%, IGBP = 0.75%, MODIS = 0.08%. Although the omission error seems overwhelming for every algorithm, a large part of it was due to low fire pixel sampling rate caused by limited satellite overpass frequency (once during the day), and made worse by cloud cover. On the other hand, the commission

errors seem small because only errors in the forested areas were considered in the overall accuracy estimates. Moreover, the area of misidentified pixels for each algorithm was expressed as a proportion of the vast unburned forest area in the ground-surveyed provinces. Nevertheless, if the number of misidentified pixels for each algorithm is expressed as a fraction of the total number of pixels flagged by it, the 'proportional' commission errors would be CCRS=30%, ESA=21%, GIGLIO=59%, IGBP=50%, MODIS=22%. These values show the level of contamination of detected fires by false alarms in forested areas. The situation is even worse in non-forest areas, as it was found that for each algorithm, most commission errors occurred in the Canadian agricultural and prairie zone on very hot days (heat wave). Comparatively, although the ESA and MODIS algorithms produced the highest omission errors due to their relatively higher thresholds, they at the same time gave the lowest commission errors. The CCRS algorithm gave the overall best performance, probably because it was developed primarily for Canadian regional application. The type of algorithm (fixed threshold or contextual) does not appear to have influenced their relative performance.

Detailed analysis of the algorithms and data show that they both have significant weaknesses that limit the fire detection accuracy. Both the fixed-threshold and contextual algorithms are based on a series of tests employing thresholds that may have been determined either through modelling or empirically using data samples that may not be adequately representative in spatial or temporal coverage. As such, the relative performance of each algorithm is dependent on land-cover type. Therefore, it is obvious that none of the AVHRR-based algorithms can produce the same performance in all environments. Although AVHRR data may have been very useful for global vegetation assessment and monitoring, and to some extent also for fire detection, its applicability for fire detection is limited due to several factors. First, fire detection was not part of the considerations during the AVHRR instrument conception. Second, the instrument has only five spectral bands with low spectral (bandwidth) and radiometric (dynamic range) resolutions. Therefore, it does not always express fire characteristics adequately. Improvement in algorithm may not lead to any significant improvement in detection accuracy globally. But by adapting algorithms to specific regional contexts, much accuracy improvement could be achieved regionally.

MODIS offers considerable advantages in data characteristics. It has 36 spectral channels with much higher spectral and radiometric (and in some cases even spatial) resolutions. The original MODIS fire algorithm used in this study was conceived around the AVHRR data concept. MODIS data is currently being characterized, and the operational fire algorithm is being modified based on experiences with actual MODIS data (Justice *et al.* 2002). This is aimed at attaining optimal capability in global fire detection.

Forest Service) and Shane Chetner (Conservation and Development Branch, Alberta Agriculture, Food and Rural Development) for providing the meteorological time series data and plots for Medicine Hat.

## References

ANDREAE, M. O., FISHMAN, J., GARSTANG, M., GOLDAMMER, J. G., JUSTICE, C. O., LEVINE, J. S., SCHOLES, R. J., STOCKS, B. J., THOMPSON, A. M., VAN WILGEN, B. W., and the STARE/TRACE-A/SAFARI Science Team, 1994, Biomass burning in the global environment: First results from the IGAC/BIBEX field campaign STARE/TRACE-A/SAFARI-92. In *Global Atmospheric-Biospheric Chemistry,* edited by R. G. Prinn (New York: Plenum), pp. 83–101.

ARINO, O., MELINOTTE, J.-M., and CALABRESI, G., 1993, Fire, cloud, land, water: the 'Ionia' AVHRR CD-browser of ESRIN. *Earth Observation Quarterly*, **41**, 6–7.

BOLES, S. H., and VERBYLA, D. L., 2000, Comparison of three AVHRR-based fire detection algorithms for interior Alaska. *Remote Sensing of Environment*, **72**, 1–16.

CIHLAR, J., and TEILLET, P.M., 1995, Forward piecewise linear model for quasi-real time processing of AVHRR data. *Canadian Journal for Remote Sensing* **21**, 22–27.

CIHLAR, J., CHEN, J., LI, Z., LATIFOVIC, R., FEDOSEJEVS, G., ADAIR, M., PARK, W., FRASER, R., TRISHCHENKO, A., GUINDON, B., STANLEY, D., and MORSE, D., 2002, GeoComp–N, An advanced system for the processing of coarse and medium resolution satellite data. Part 2: biophysical products for northern ecosystems. *Canadian Journal of Remote Sensing*, **28**, 21–44.

CUOMO, V., LASAPONARA, R., and TRAMUTOLI, V., 2001, Evaluation of a new satellite-based method for forest fire detection. *International Journal of Remote Sensing*, **22,** 1799–1826.

FLASSE, S. P., and CECCATO, P., 1996, A contextual algorithm for AVHRR fire detection. *International Journal of Remote Sensing*, **17**, 419–424.

FRANCA, J. R. A., BRUSTET, J. M., and FONTAN, J., 1995, Multispectral remote sensing of biomass burning in West Africa. *Journal of Atmospheric Chemistry*, **22**, 81–110.

FRASER, R.H., LI, Z., and CIHLAR, J., 2000, Hotspot and NDVI Differencing Synergy (HANDS): a new technique for burned area mapping over boreal forest. *Remote Sensing of Environment*, **74**, 362–376.

GIGLIO, L., KENDALL, J. D., and JUSTICE, C. O., 1999, Evaluation of global fire detection algorithms using simulated AVHRR infrared data. *International Journal of Remote Sensing*, **20**, 1947–1985.

GIGLIO, L., KENDALL, J. D., and TUCKER, C. J., 2000, Remote sensing of fires with the TRMM VIRS. *International Journal of Remote Sensing*, **21**, 203–207.

JUSTICE, C. O., and DOWTY, P. (editors), 1994, IGBP-DIS satellite fire detection algorithm workshop technical report. *IGBP-DIS Working Paper 9,* NASA/ GSFC, Greenbelt, MD, February 1993.

JUSTICE, C. O., and MALINGREAU, J.-P. (editors), 1996, The IGBP-DIS fire algorithm workshop 2. *IGBP-DIS Working Paper 14*, Ispra, Italy, October 1995.

JUSTICE C. O., GIGLIO L., KORONTZI, S., OWENS, J., MORISETTE, J. T., ROY, D., DESCLOITRES, J., ALLEAUME, S., PETITECOLIN, F., and KAUFMAN, Y., 2002, The MODIS fire products. *Remote Sensing of Environment*, (in press).

JUSTICE, C. O., KENDALL, J. D., DOWTY, P. R., and SCHOLES, R. J., 1996, Satellite remote sensing of fires during the SAFARI campaign using NOAA-AVHRR data. *Journal of Geophysical Research*, **101**, 23 851–23 863.

JUSTICE, C. O., MALINGREAU, J.-P., and SETZER, A. W., 1993, Satellite remote sensing of fires: potential and limitations. In *Fire in the Environmen*t, edited by P. J. Crutzen and J. G. Goldammer (New York: John Wiley), pp. 77–88.

KAUFMAN, Y. J., JUSTICE, C. O., FLYNN, L. P., KENDALL, J. D., PRINS, E. M., GIGLIO, L., WARD, D. E., MENZEL, W. P., and SETZER, A. W., 1998, Potential global fire monitoring from EOS-MODIS. *Journal of Geophysical Research*, **103**, 32 215–32 238.

KAUFMAN, Y. J., TUCKER, C. J., and FUNG, I., 1990, Remote sensing of biomass burning in the tropics. *Journal of Geophysical Research*, **95**, 9927–9939.

Kennedy, P. J., Belward, A. S., and Gregoire, J.-M., 1994, An improved approach to fire monitoring in West Africa using AVHRR data. *International Journal of Remote Sensing*, **15**, 2235–2255.

Kidwell, K. B. (editor), 1998, *NOAA Polar Orbiter Data User's Guide.* US Department of Commerce, NESDIS, NOAA, National Climatic Data Centre, Satellite Data Services Division, Washington, DC, USA.

Li, Z., Kaufman, Y. J., Ichoku, C., Fraser, R., Trishchenko, A., Giglio, L., Jin, J., and Yu, X., 2001, A review of AVHRR-based active fire detection algorithms: principles, limitations, and recommendations. In *Global and Regional Vegetation Fire Monitoring from Space: Planning and coordinated international effort,* edited by F. Ahern, J. G. Goldammer, and C. Justice (The Hague: SPB Academic Publishing), pp. 199–225.

Li, Z., Nadon, S., and Cihlar, J., 2000a, Satellite-based detection of Canadian boreal forest fires: development and application of the algorithm. *International Journal of Remote Sensing*, **21**, 3057–3069.

Li, Z., Nadon, S., Cihlar, J., and Stocks, B., 2000b, Satellite-based mapping of Canadian boreal forest fires: evaluation and comparison of algorithms. *International Journal of Remote Sensing*, **21**, 3071–3082.

Nakayama, M., Maki, M., Elvidge, C. D., and Liew, S. C., 1999, Contextual algorithm adapted for NOAA-AVHRR fire detection in Indonesia. *International Journal of Remote Sensing*, **20**, 3415–3421.

Pokrant, H., 1991, Land cover map of Canada derived from AVHRR images. Manitoba Remote Sensing Centre, Winnipeg, Manitoba, Canada.

Pozo, D., Olmo, F. J., and Alados-Arboledas, L., 1997, Fire detection and growth monitoring using a multitemporal technique on AVHRR mid-infrared and thermal channels. *Remote Sensing of Environment*, **60**, 111–120.

Prins, E., and Menzel, W. P., 1992, Geostationary satellite detection of biomass burning in South America. *International Journal of Remote Sensing*, **13**, 2783–2799.

Rao, C. R. N., and Chen, J., 1996, Post-launch calibration of the visible and near-infrared channels of the Advanced Very High Resolution Radiometer on NOAA-14 spacecraft. *International Journal of Remote Sensing*, **17**, 2743–2747.

Rauste, Y., Herland, E., Frelander, H., Soini, K., Kuoremaki, T., and Ruokari, A., 1997, Satellite-based forest fire detection for fire control in boreal forests. *International Journal of Remote Sensing*, **18**, 2641–2656.

Robertson, B., Erickson, A., Friedel, J., Guindon, B., Fisher, T., Brown, R., Teillet, P., D'Iorio, M., Cihlar, J., and Sancz, A., 1992, GEOCOMP, a NOAA AVHRR geo-coding and compositing system. *Proceedings of the ISPRS Conference, Commission 2, Washington, DC, 2–14 August 1992* (Washington: ISPRS), pp. 223–228.

Serway, R. A., 1992, *Physics for Scientists and Engineers*, 3rd edn (Philadelphia, PA: Saunders College Publishing).

Trishchenko, A., and Li, Z., 2001, A method for the correction of AVHRR onboard IR calibration in the event of short-term radiative contamination. *International Journal of Remote Sensing*, **22**, 3619–3624.